A

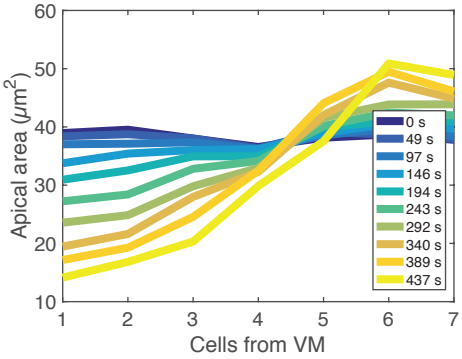

B

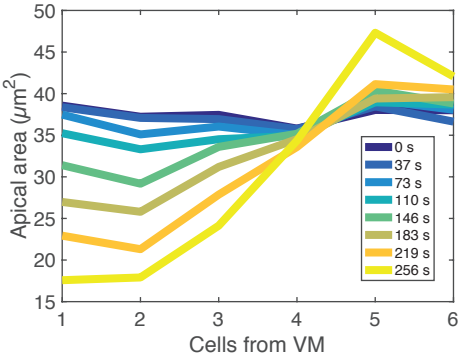

C

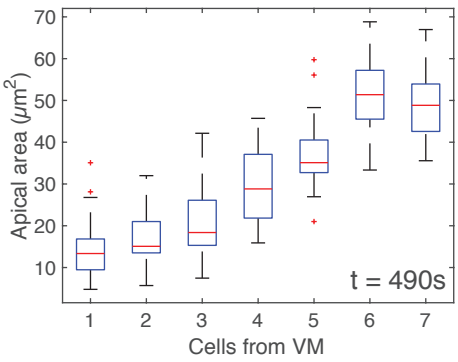

D

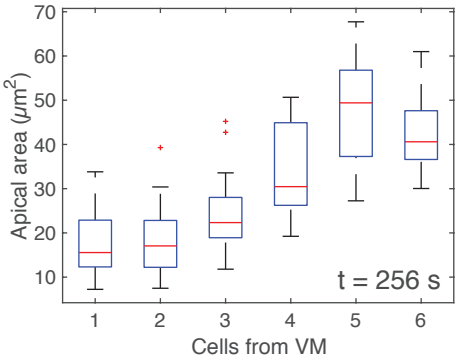

E

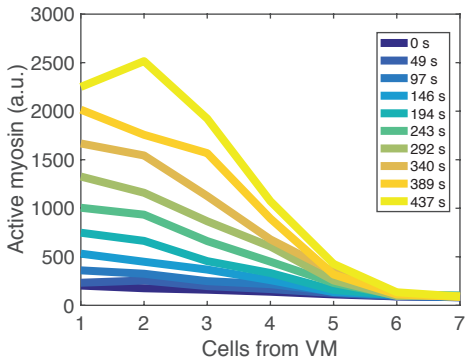

F

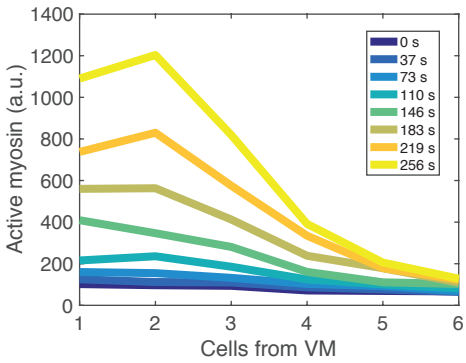

G

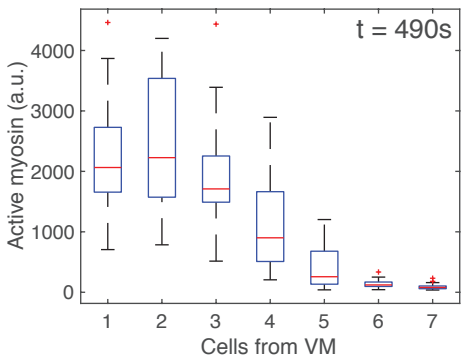

H

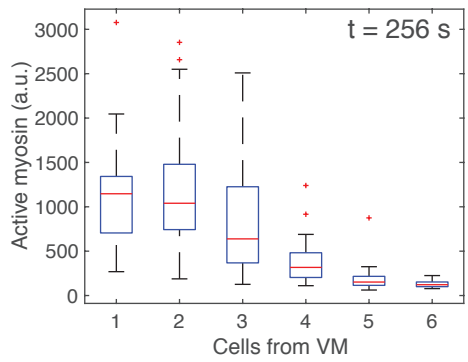

I

Cells from VM	1	2	3	4	5	6	7
1	1.00	0.26	0.17	0.00	0.00	0.00	0.00
2	0.26	1.00	0.17	0.00	0.00	0.00	0.00
3	0.17	0.17	1.00	0.04	0.00	0.00	0.00
4	0.00	0.00	0.04	1.00	0.04	0.00	0.00
5	0.00	0.00	0.00	0.04	1.00	0.00	0.00
6	0.00	0.00	0.00	0.00	0.00	1.00	0.00
7	0.00	0.00	0.00	0.00	0.00	0.00	1.00

J

Cells from VM	1	2	3	4	5	6
1	1.00	0.60	0.00	0.00	0.00	0.00
2	0.60	1.00	0.02	0.00	0.00	0.00
3	0.00	0.02	1.00	0.00	0.00	0.00
4	0.00	0.00	0.00	1.00	0.00	0.00
5	0.00	0.00	0.00	0.00	1.00	0.30
6	0.00	0.00	0.00	0.00	0.30	1.00

Fig. S1. Apical area and active myosin intensity are present in a ventral-lateral gradient in two additional WT embryos. (A) and (B) Apical constriction is graded along the ventral-lateral axis in WT embryos. Apical area (y-axis) is plotted for each cell position bin (x-axis) for each time frame (colorbar) as each embryo furrows. (C) and (D) Distribution of cell areas for cell bin at a late time point highlights the gradient at t = 406s (C) and t=256s (D). (E) and (F) Increase in total active myosin intensity per cell is graded along the ventral-lateral axis. Average total apical myosin intensity per cell (y-axis) is plotted for each cell position bin (x-axis) for each time frame (colorbar). (G) and (H) Distribution of levels of active myosin per cell for each cell bin show a gradient in the average cell behavior at t=406s (G) and t = 256s (H). (I) and (J) Statistical significance of pairwise comparisons between distributions of active myosin levels in cell bins at different positions from the VM. (C, D, G, and H) Gradients depicted as a box and whisker plot at t=406s. Red lines indicate median values, box indicates inner quartiles, dotted lines indicate outer quartiles. (I - J) Tables show p-values from a two-sample Kolmogorov-Smirnov (K-S) test comparing the distribution of active myosin in each cell bin with each other cell bin for each embryo. Green shading indicates statistical significance with $p<0.05$. (A, C, E, G, and I) are measurements from one WT embryo and all cells are binned the same for each graph (A and E) n varies for each cell bin and time point. n = 15 cells/bin (minimum) and 48 cells/bin (average). (C, G, and I) n for cell bins 1-7 at t = 490 s is 39, 23, 19, 15, 17, 32, and 36 respectively (B, D, F, H, and J) are measurements from a second WT embryo and all cells are binned the same for each graph (B,F) n varies for each cell bin and time point. n = 13 cells/bin (minimum) and 42 cells/bin (average). (D, H, and J) n for cell bins 1-6 at t = 256 s are 53, 37, 30, 23, 17, and 13 respectively.

A

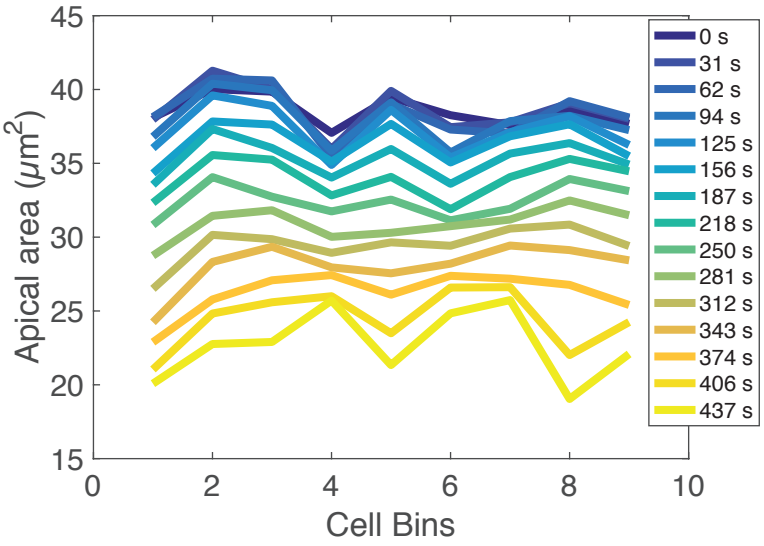

B

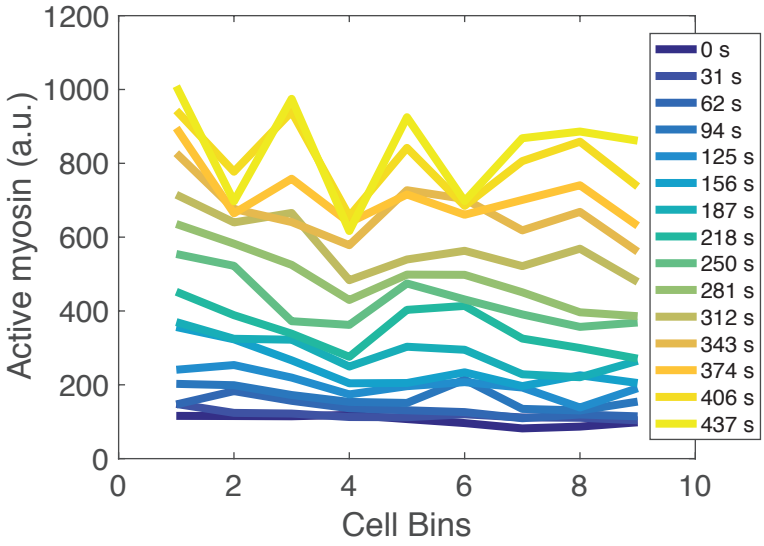

C

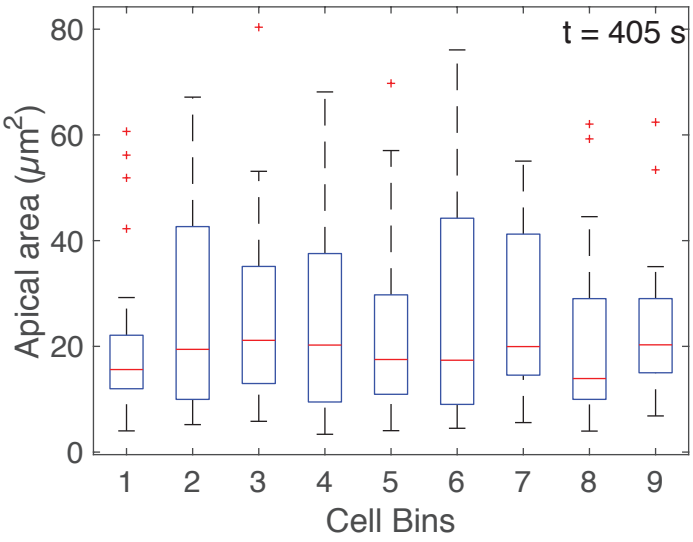

D

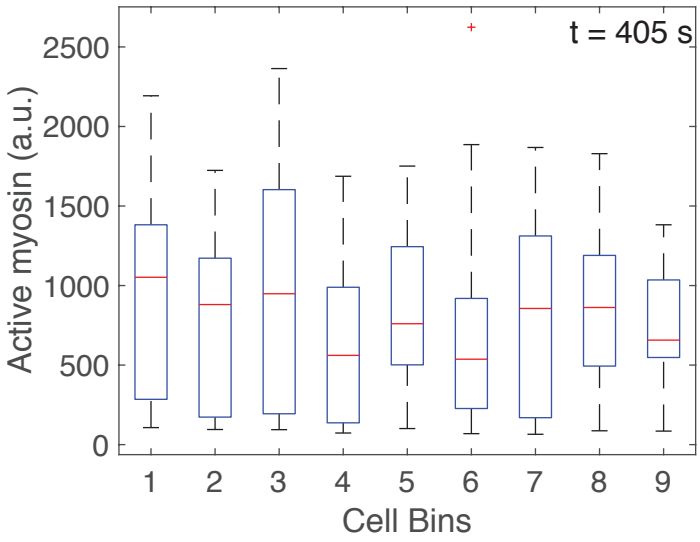

E

Cell Bins	1	2	3	4	5	6	7	8	9
1	1.00	0.64	0.77	0.20	0.83	0.02	0.52	0.59	0.14
2	0.64	1.00	0.80	0.92	0.79	0.17	0.99	0.77	0.86
3	0.77	0.80	1.00	0.32	0.42	0.08	0.67	0.75	0.32
4	0.20	0.92	0.32	1.00	0.20	0.89	0.78	0.20	0.27
5	0.83	0.79	0.42	0.20	1.00	0.26	0.32	0.93	0.58
6	0.02	0.17	0.08	0.89	0.26	1.00	0.50	0.26	0.21
7	0.52	0.99	0.67	0.78	0.32	0.50	1.00	0.49	0.60
8	0.59	0.77	0.75	0.20	0.93	0.26	0.49	1.00	0.59
9	0.14	0.86	0.32	0.27	0.58	0.21	0.60	0.59	1.00

F

Cell Bins	1	2	3	4	5	6	7	8	9
1	1.00	0.49	0.32	0.84	0.49	0.76	0.28	0.59	0.16
2	0.49	1.00	0.33	0.94	0.70	0.98	0.13	0.96	0.04
3	0.32	0.33	1.00	0.94	0.84	0.40	0.64	0.34	0.79
4	0.84	0.94	0.94	1.00	0.87	0.94	0.70	0.59	0.41
5	0.49	0.70	0.84	0.87	1.00	0.57	0.59	0.72	0.40
6	0.76	0.98	0.40	0.94	0.57	1.00	0.13	0.77	0.04
7	0.28	0.13	0.64	0.70	0.59	0.13	1.00	0.22	0.39
8	0.59	0.96	0.34	0.59	0.72	0.77	0.22	1.00	0.06
9	0.16	0.04	0.79	0.41	0.40	0.04	0.39	0.06	1.00

Fig. S2. Apical area and apical myosin do not exhibit a gradient along the anterior-posterior (A-P) axis. (A) Apical area in a wild-type embryo (same as in Fig. 1) does not exhibit a gradient along the A-P axis. Apical area (y-axis) is plotted for each cell bin at different positions along A-P axis (x-axis) for each time frame (colorbar) as the embryo furrows. (B) Apical myosin is also not in a gradient along the A-P axis. Average total apical myosin intensity per cell (y-axis) is plotted for each cell position bin (x-axis) for each time frame (colorbar). (C) and (D) the distribution of apical cells area (C) and active myosin (D) at t = 405 s. Red lines indicate median values, box indicates inner quartiles, while dotted lines indicate outer quartiles. (E) Apical area distributions at t = 405 s are not statistically different from each other. (F) Active myosin distributions at t = 405 s are for the most part not significantly different from each other. (E) and (F) Tables show p-values from a two-sample Kolmogorov-Smirnov (K-S) test comparing the distribution of apical area (E) and active myosin (F) between each pair of cell bins. Green shading indicates statistical significance with $p<0.05$. (A - F) are measurements from the same embryo as in Fig. 1 and binning was performed the same for all measurements. n varies for each cell bin and time point. n = 19 cells/bin (minimum) and 26 cells/bin (average). (C - F) n for cell bins 1 - 9 at t = 405 s are 23, 22, 26, 23, 27, 22, 19, 23, and 21 respectively.

A

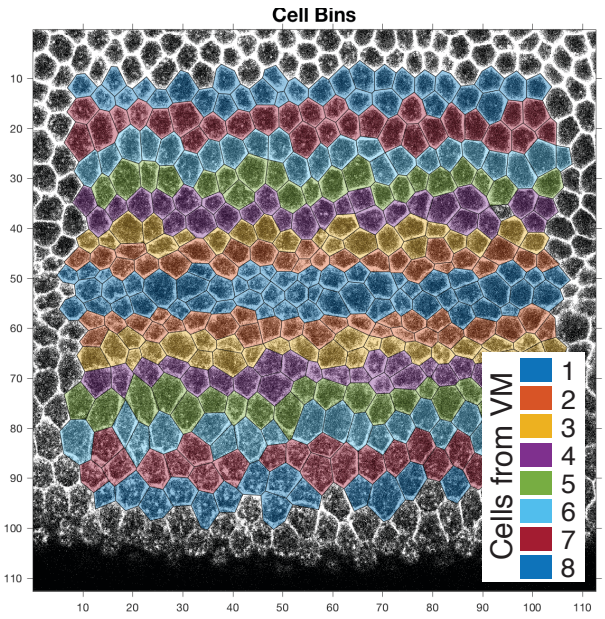

B

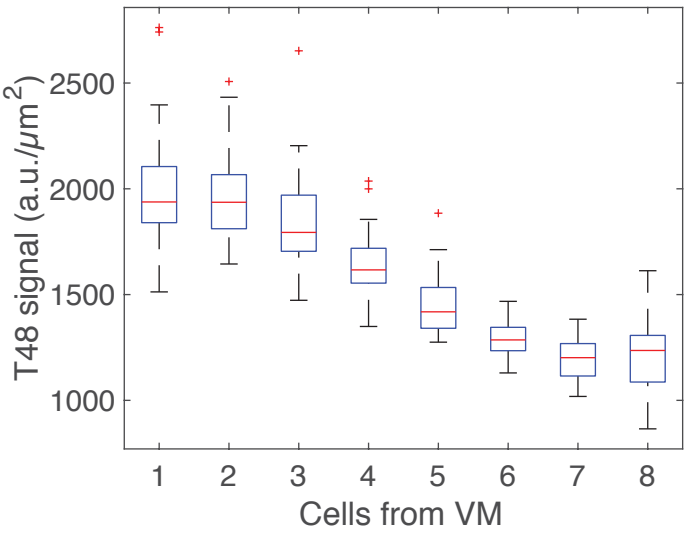

C

Cells from VM	1	2	3	4	5	6	7	8
1	1.00	0.59	0.00	0.00	0.00	0.00	0.00	0.00
2	0.59	1.00	0.01	0.00	0.00	0.00	0.00	0.00
3	0.00	0.01	1.00	0.00	0.00	0.00	0.00	0.00
4	0.00	0.00	0.00	1.00	0.00	0.00	0.00	0.00
5	0.00	0.00	0.00	0.00	1.00	0.00	0.00	0.00
6	0.00	0.00	0.00	0.00	0.00	1.00	0.00	0.01
7	0.00	0.00	0.00	0.00	0.00	0.00	1.00	0.10
8	0.00	0.00	0.00	0.00	0.00	0.01	0.10	1.00

D

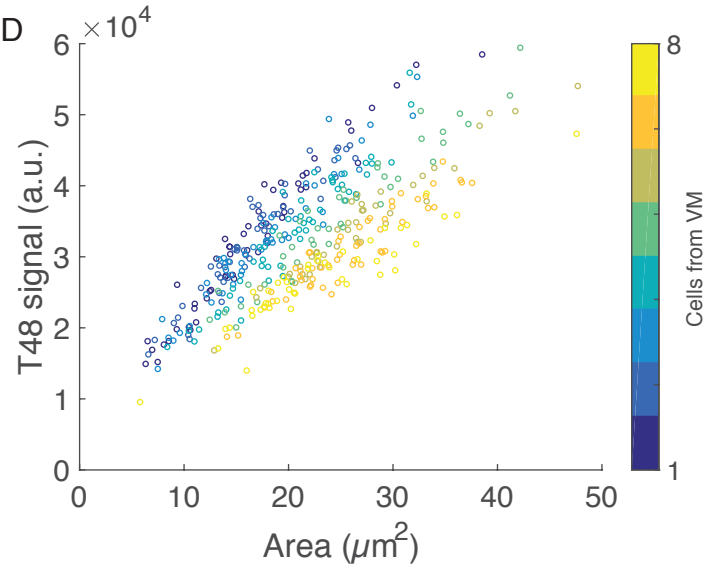

Fig. S3. T48::GFP signal density exhibits graded levels 3 – 7 cells from VM in a second T48::GFP expressing embryo. (A) Cell bins as manually determined in fixed embryo. Images show cell outlines (phalloidin stain). Cells are color coded by the bin in which they are measured. Colors repeat after 7 bins. (B) Average T48 signal density is graded along the ventral-lateral axis with highest levels at the VM. GFP::T48 density (fluorescence intensity μm^{-2}) (y-axis) as a function of cells from the VM (x-axis) (See (A) for illustration of cell bins. (C) A statistically significant gradient in T48 levels is observed from 2-7 cells from the VM. Table of p-values generated from a two-sample K-S test comparing the distribution of T48 (a.u. per μm^2) in each cell bin with each other cell bin. Green shading indicates statistical significance with $p<0.05$. (D) Total GFP::T48 signal per cell is higher in cells closer to the VM for a given cell area. Total GFP::T48 signal per cell (y-axis) as a function of apical cell area (x-axis). Cell bin is denoted (colorbar). (B-D) show measurements from a single embryo different from the embryo in Fig. 2. n of cells for each bins 1 - 8 are 53, 52, 49, 50, 43, 42, 51, and 45, respectively.

A

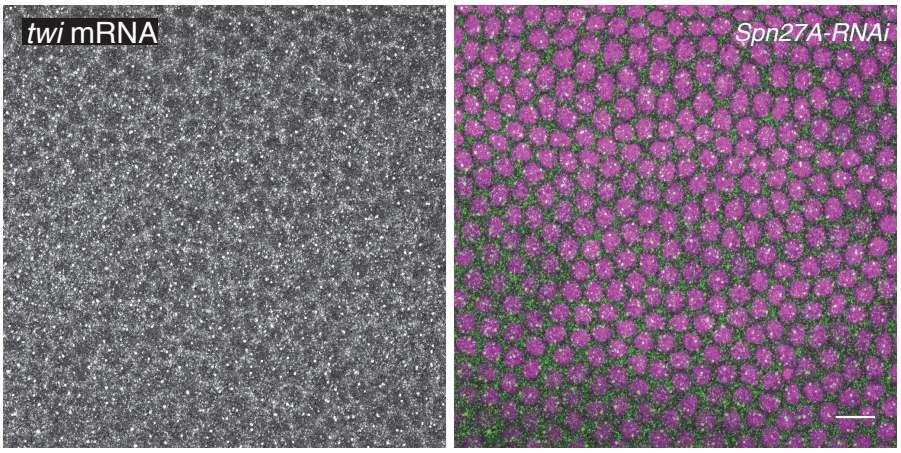

B

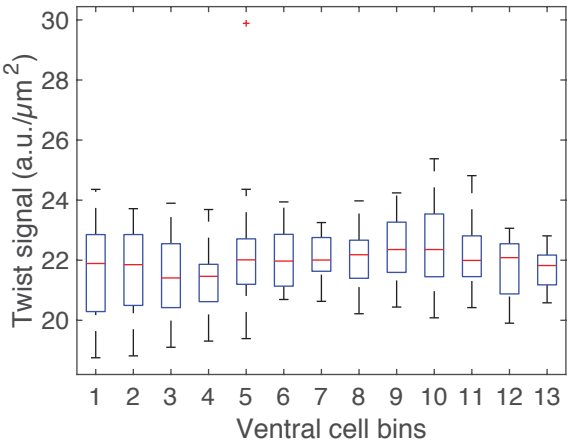

C

Ventral cell bins	1	2	3	4	5	6	7	8	9	10	11	12	13
1	1.00	0.95	0.82	0.04	0.07	0.08	0.13	0.35	0.26	0.28	0.28	0.55	0.13
2	0.95	1.00	0.80	0.09	0.22	0.13	0.29	0.47	0.36	0.30	0.42	0.75	0.13
3	0.82	0.80	1.00	0.15	0.06	0.05	0.08	0.23	0.13	0.18	0.07	0.35	0.08
4	0.04	0.09	0.15	1.00	0.02	0.07	0.05	0.02	0.00	0.01	0.10	0.06	0.15
5	0.07	0.22	0.06	0.02	1.00	0.99	0.63	0.89	0.36	0.47	0.93	0.88	0.37
6	0.08	0.13	0.05	0.07	0.99	1.00	0.89	0.92	0.67	0.64	0.96	0.59	0.44
7	0.13	0.29	0.08	0.05	0.63	0.89	1.00	0.98	0.27	0.48	0.94	0.91	0.71
8	0.35	0.47	0.23	0.02	0.89	0.92	0.98	1.00	0.30	0.69	0.98	0.93	0.30
9	0.26	0.36	0.13	0.00	0.36	0.67	0.27	0.30	1.00	0.74	0.54	0.13	0.02
10	0.28	0.30	0.18	0.01	0.47	0.64	0.48	0.69	0.74	1.00	0.57	0.50	0.14
11	0.28	0.42	0.07	0.10	0.93	0.96	0.94	0.98	0.54	0.57	1.00	0.90	0.71
12	0.55	0.75	0.35	0.06	0.88	0.59	0.91	0.93	0.13	0.50	0.90	1.00	0.57
13	0.13	0.13	0.08	0.15	0.37	0.44	0.71	0.30	0.02	0.14	0.71	0.57	1.00

Fig. S4. *twist* mRNA expression is uniform around the VM in a *Spn27A-RNAi* embryo. (A) *twist* mRNA at early nuclear cycle 14 in a *Spn27A-RNAi* embryo. Images are single z-slices, *en face*, at the level of the nuclei. Left image shows *twist* mRNA staining and right image is a merge of the *twist* mRNA in green and DAPI in magenta (B) Cytoplasmic *twist* mRNA signal is uniform around the VM. Cytoplasmic *twist* mRNA signal (fluorescence intensity/μm^2) is plotted as a function of cells from the VM (x-axis)(determined by average cell diameter). (C) There is no statistically significant gradient in levels of *twist* mRNA. Table of p-values generated from a two-sample k-s test comparing the distribution of *twist* (a.u. μm^{-2}) in each cell bin with each other cell bin. Green shading indicates statistical significance with $p<0.05$. Data from one embryo is presented. n of cells for each bin (1-13) is 23, 16, 19, 22, 21, 21, 21, 23, 20, 23, 19, 19, and 20 respectively. Scale bars = 10 μm

A

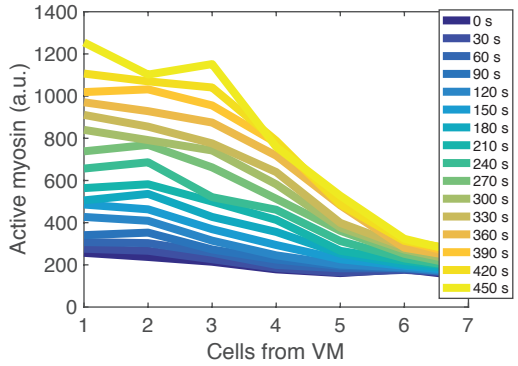

B

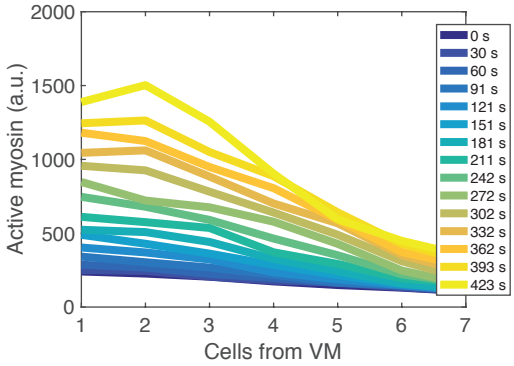

C

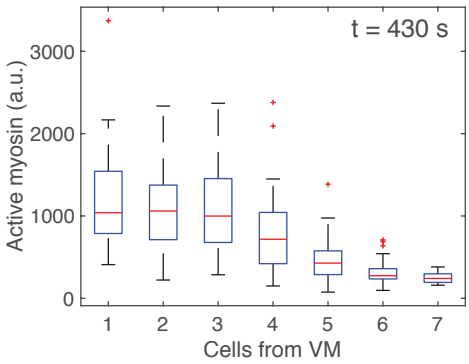

D

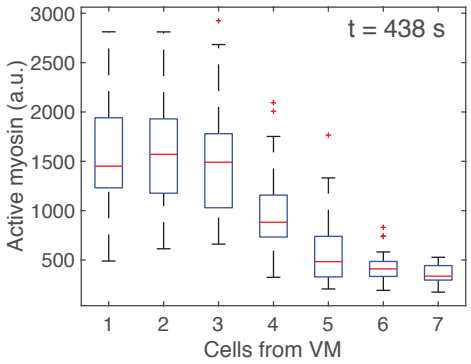

E

Cells from VM

Cells from VM	1	2	3	4	5	6	7
1	1.00	0.60	0.82	0.00	0.00	0.00	0.00
2	0.60	1.00	0.75	0.00	0.00	0.00	0.00
3	0.82	0.75	1.00	0.02	0.00	0.00	0.00
4	0.00	0.00	0.02	1.00	0.00	0.00	0.00
5	0.00	0.00	0.00	0.00	1.00	0.01	0.00
6	0.00	0.00	0.00	0.00	0.01	1.00	0.12
7	0.00	0.00	0.00	0.00	0.00	0.12	1.00

F

Cells from VM

Cells from VM	1	2	3	4	5	6	7
1	1.00	0.97	0.73	0.00	0.00	0.00	0.00
2	0.97	1.00	0.90	0.00	0.00	0.00	0.00
3	0.73	0.90	1.00	0.00	0.00	0.00	0.00
4	0.00	0.00	0.00	1.00	0.00	0.00	0.00
5	0.00	0.00	0.00	0.00	1.00	0.00	0.03
6	0.00	0.00	0.00	0.00	0.00	1.00	0.12
7	0.00	0.00	0.00	0.00	0.03	0.12	1.00

G

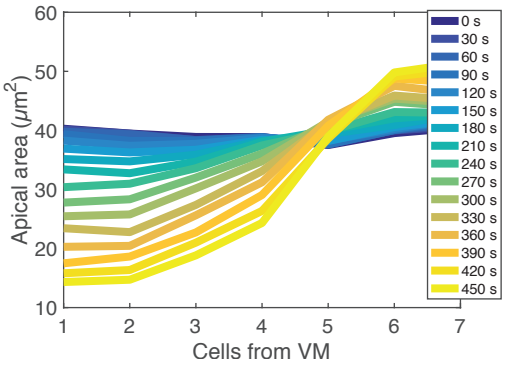

H

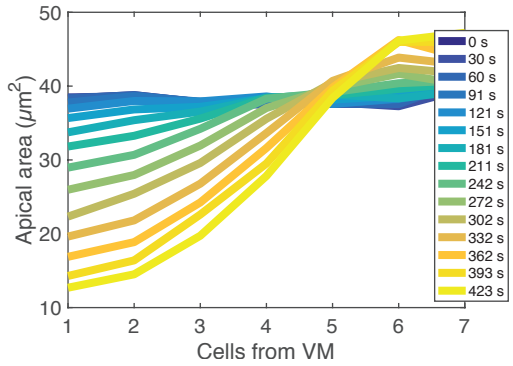

I

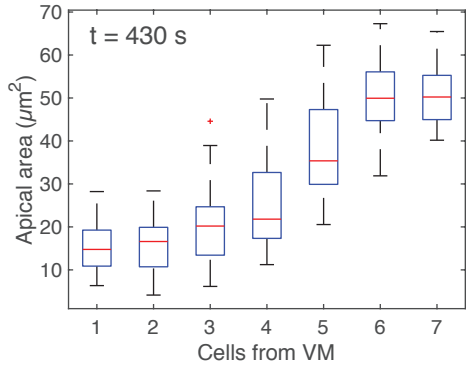

J

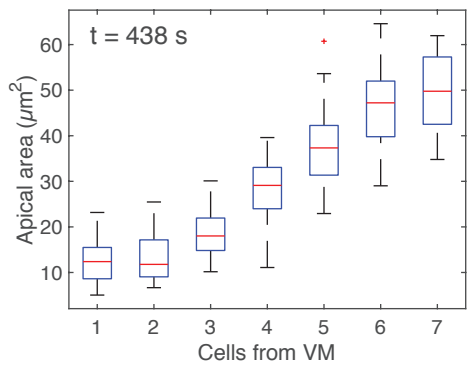

Fig. S5. Apical area and active myosin intensity are present in a ventral-lateral gradient in two *rh3-RNAi* embryos. (A) and (B) Increase in total active myosin intensity per cell is graded along the ventral-lateral axis in *rhodopsin-3-RNAi* (control) embryos. Average total apical myosin intensity per cell (y-axis) is plotted for each cell position bin (x-axis) for each time frame (colorbar). (C) and (D) Distribution of levels of active myosin per cell for each cell bin show a gradient in the average cell behavior at t=430 s (C) and t = 438 s (D). (E) and (F) Statistical significance of pairwise comparisons between distributions of active myosin levels in cell bins at different positions from the VM from (C) and (D) respectively. Tables show p-values from a two-sample Kolmogorov-Smirnov (K-S) test comparing the distribution of active myosin in each cell bin with each other cell bin for each embryo. Green shading indicates statistical significance with $p<0.05$. (G) and (H) Apical constriction is graded along the ventral-lateral axis in WT embryos. Apical area (y-axis) is plotted for each cell position bin (x-axis) for each time frame (colorbar) as each embryo furrows. (I) and (J) Distribution of cell areas for cell bin at a late time point highlights the gradient at t = 430 s (I) and t=438 s (J). (A, C, E, G, and I) are measurements from one *rh3-RNAi* embryo. (A, G) n varies for each cell bin and time point. n = 26 cells/bin (minimum) and 49 cells/bin (average). (C, E, and I) n for cell bins 1-7 at t = 430 s is 53, 51, 48, 56, 36, 3, and 27, respectively (B, D, F, H, and J) are measurements from a second WT embryo. (B and H) n varies for each cell bin and time point. n = 10 cells/bin (minimum) and 53 cells/bin (average). (D, H, and J) n for cell bins 1-7 at t = 438 s is 35, 30, 33, 37, 48, 40, and 10, respectively.

A

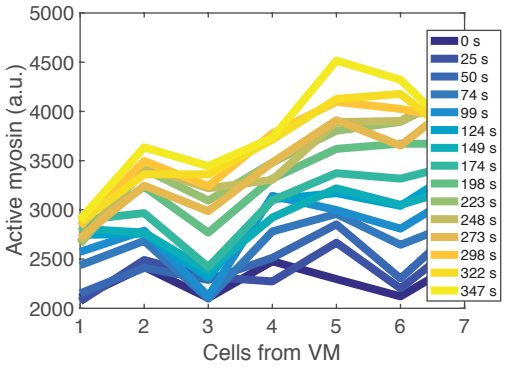

B

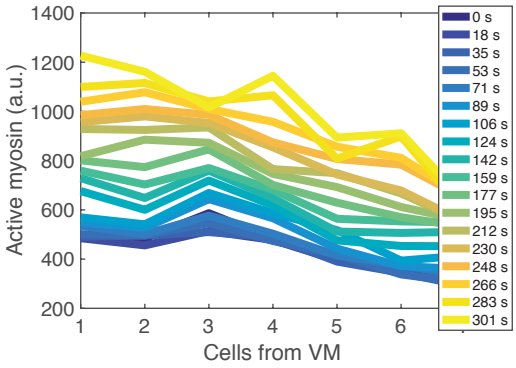

C

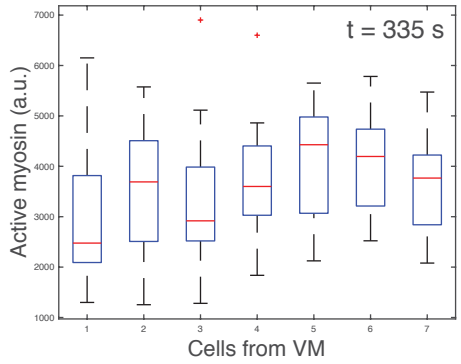

D

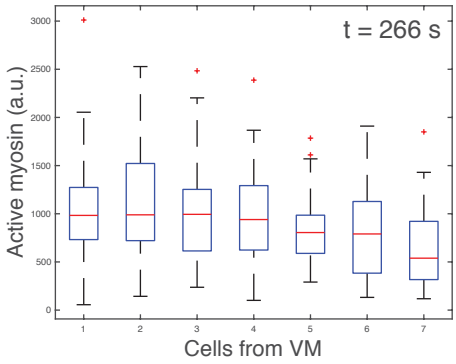

E

Cells from VM

Cells from VM	1	2	3	4	5	6	7
1	1.00	0.02	0.05	0.00	0.00	0.00	0.03
2	0.02	1.00	0.19	0.68	0.52	0.40	0.69
3	0.05	0.19	1.00	0.05	0.05	0.00	0.19
4	0.00	0.68	0.05	1.00	0.25	0.35	0.76
5	0.00	0.52	0.05	0.25	1.00	0.93	0.08
6	0.00	0.40	0.00	0.35	0.93	1.00	0.21
7	0.03	0.69	0.19	0.76	0.08	0.21	1.00

F

Cells from VM

Cells from VM	1	2	3	4	5	6	7
1	1.00	0.50	0.53	0.42	0.07	0.08	0.00
2	0.50	1.00	0.32	0.45	0.05	0.17	0.00
3	0.53	0.32	1.00	0.81	0.04	0.48	0.01
4	0.42	0.45	0.81	1.00	0.47	0.48	0.01
5	0.07	0.05	0.04	0.47	1.00	0.60	0.03
6	0.08	0.17	0.48	0.48	0.60	1.00	0.32
7	0.00	0.00	0.01	0.01	0.03	0.32	1.00

G

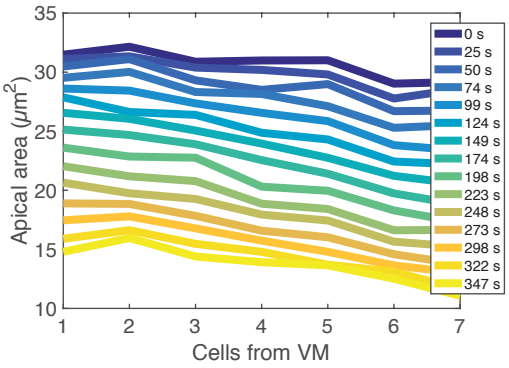

H

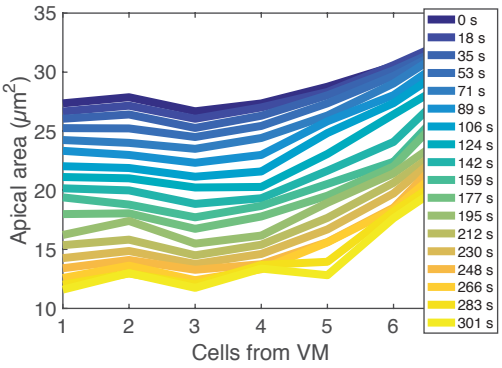

I

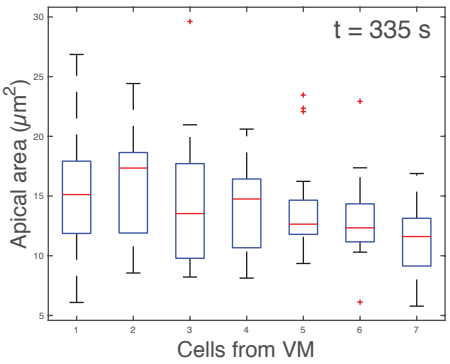

J

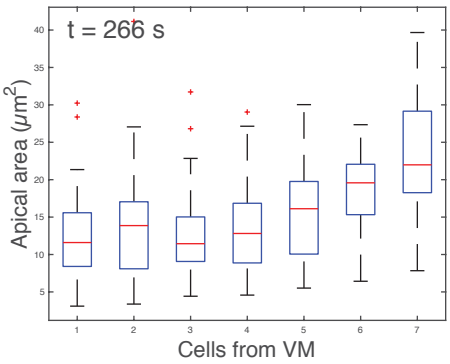

Fig. S6. *Spn27A-RNAi* shows that the active myosin gradient is dependent on *dorsal* patterning in two additional *Spn27A--RNAi* embryos. (A) and (B) *Spn27A-RNAi* results in relatively uniform active myosin levels along ventral-lateral axis at all time points in two different embryos. Plot shows average active myosin intensity for each bin as a function of distance from VM. Different color lines are different time points. (C) and (D) The distribution of active myosin in two different embryos at t = 335 s and t = 266 s respectively. The distribution for each bin is depicted as a box and whisker plot. Red lines indicate median values, box indicates inner quartiles, while dotted lines indicate outer quartiles. (E) and (F) Active myosin neither embryo has a statistically significant gradient in average active myosin. Table of p-values generated from a two-sample K-S test comparing the distribution of active myosin (fluorescence intensity) in each cell bin with each other cell bin for the data plotted in (C) and (D) respectively. Green shading indicates statistical significance with $p<0.05$. (G) and (H) *Spn27A-RNAi* results in uniform apical constriction along ventral-lateral axis in two separate embryos. Plot shows average apical area for each bin. Different color lines are different time points. (G) The distribution of apical area in two different embryos at t = 335 s and t = 266 s respectively. The distribution for each bin is depicted as a box and whisker plot. Red lines indicate median values, box indicates inner quartiles, while dotted lines indicate outer quartiles. (H) (A, C, E, G, and I) are measurements from a single embryo. Binning was performed the same for all measurements. (A) and (G) n varies for each cell bin and time point. n = 12 cells/bin (minimum) and 22 cells/bin (average). (C, E, and I) n for cell bins 1-7 at t = 335 s are 38, 18, 21, 19, 19, 20, and 12 respectively. (B, D, F, H, and J) are measurements from a single embryo. Binning was performed the same for all measurements. (B) and (H) n varies for each cell bin and time point. n = 21 cells/bin (minimum) and 62 cells/bin (average). (D, F, and J) n for cell bins 1-7 at t = 266 s are 59, 60, 61, 47, 31, 24, and 29 respectively.

A

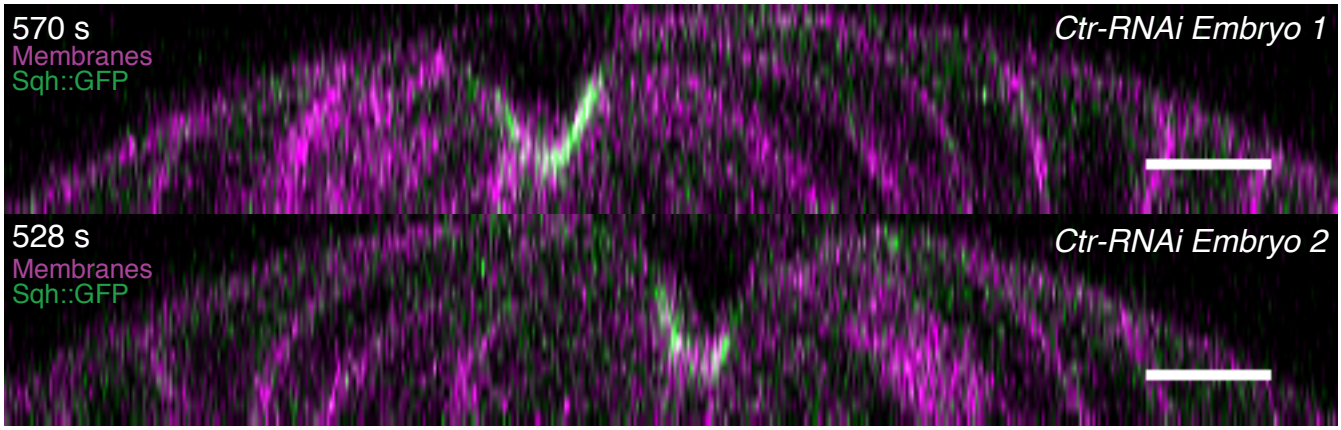

B

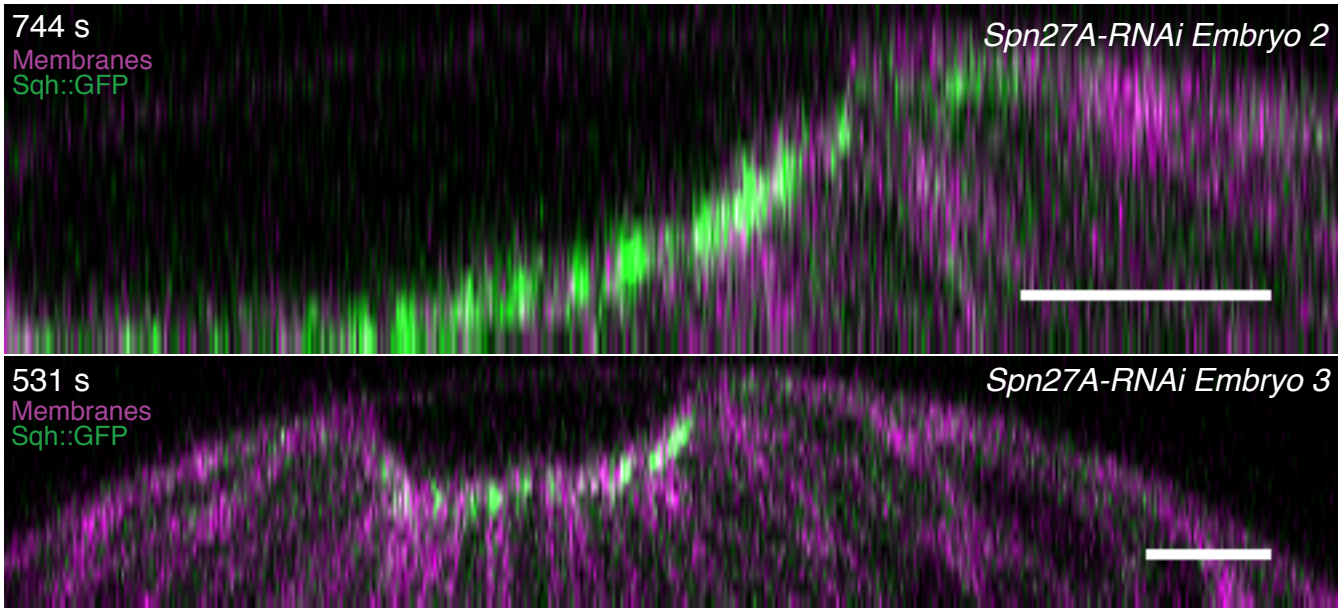

C

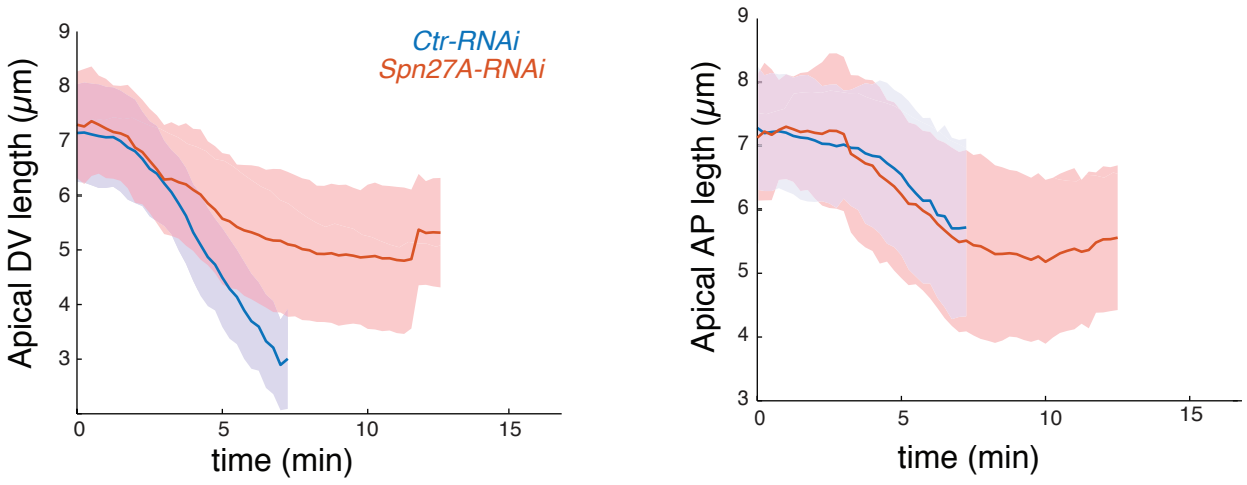

Fig. S7. **The shape of the furrow flatter in *Spn27A-RNAi* embryos than in control embryos and the apical area uniformly constricted around the VM.** (A) The cross-sectional shape of the furrow in control *rh3-RNAi* is consistent with the WT furrow shape. Z projection from an image stack from two control embryos. Embryo 1 is the same embryo as measured in Fig. S5 A, C, E, and G. Embryo 2 is the same embryo as measured in Fig. S5 B, D, F, and H. Timestamps are consistent with Fig. S5. (B) The cross-section shape of the furrow in *Spn27A-RNAi* embryos is flatter and consistent with the model. Images are Z projections from an image stack from two *Spn27A* embryos. Embryo 2 is the same embryo as measured in Fig. S6 A, C, E, and G. Embryo 3 is the same embryo as measured in Fig. S6 B, D, F, and H. (C) Quantification of apical cell length along each embryonic axis shows that control cells constrict more along the dorsal-lateral (DV) axis than *Spn27A-RNAi* embryos (left), but constrict a similar amount along the anterior-posterior (AP) axis (right). Cell length along each axis was determined by fitting an ellipsoid to shape of the cell and measuring the length along the AP and DV axes. *Ctr-RNAi* (blue, n = 168 cells, 2 embryos), *Spn27A-RNAi* (red, n = 153 cells, 2 embryos), shaded areas indicate SD.

Table S1

Stock	Genotype	Source/Reference	Figure (# of embyros)
1	SqhGFP Royou		
2	w; Gap43::mCherry(attp40); Sqh::GFP	Martin et al., 2010	
3	OreR	Bloomington Drosophila Stock Center	3 (1)
4	y[1] sc[*] v[1]; P{y[+t7.7] v[+t1.8]=TRiP.HMC03159}attP2 (Spn27A shRNA line)	TRiP center*	
5	y[1] sc[*] v[1]; P{y[+t7.7] v[+t1.8]=TRiP.GL01052}attP2 (Rh3 shRNA control line)	TRiP center*	
6	y,w; Sqh::GFP; mat15, Gap43::mCherry/(TM3, Sb[1])	Vasquez et al., 2014	
7	y,w;+; vk33{BAC GFP::T48}	this paper	2 (1); S3 (1)
	F2 embryos imaged from these crosses, using above stock numbers/genotypes. Non-balancer females were used for cages.		
	Stock # 1 x 2 (Virgins x males)		1 B-H (1); S1(2); S2 (2)
	4 x 6 (23 and 18 ºC)		6 B-F (1); S3(1); S6 (2)
	5 x 6 (23 C)		S5 (2)

*Norbert Perrimon, Harvard Medical School and Howard Hughes Medical Institute, Boston, MA

Refereces:

Martin, A.C., M. Kaschube, and E.F. Wieschaus. 2009. Pulsed contractions of an actin-myosin network drive apical constriction. *Nature* . 457:495–499.

Martin, A.C., M. Gelbart, R. Fernandez-Gonzalez, M. Kaschube, and E.F. Wieschaus. 2010. Integration of contractile forces during tissue invagination. *J. Cell Biol.* 188:735–749.

Vasquez, C.G., M. Tworoger, and A.C. Martin. 2014. Dynamic myosin phosphorylation regulates contractile pulses and tissue integrity during epithelial morphogenesis. *J. Cell Biol.* 206:435–450.

Supplementary Materials: Actomyosin-based tissue folding requires a multicellular myosin gradient

Natalie C. Heer[1], Pearson W. Miller[2], Soline Chanet[1], Norbert Stoop[2], Jörn Dunkel[2], and Adam Martin[1]

[1]Department of Biology, Massachusetts Institute of Technology, Cambridge, MA 02139, USA
[2]Department of Mathematics, Massachusetts Institute of Technology, Cambridge, MA 02139, USA

November 7, 2016

Abstract

We provide details about the theoretical model used in the Main Text. Starting from a simplified geometric picture, we show how apical myosin contraction can be linked to the generation of spontaneous curvature. We incorporate this active stress generation into the well-established Koiter shell equations [4] to obtain a mechanical continuum model describing the morphogenesis of furrow formation.

1 Vertex model for apical constriction

We address how myosin might influence an isolated piece of the membrane through use of a vertex cell model. We consider a patch of neighboring rectangular 'model' cells (Fig. 4B, Main Text). The inner and outer faces represent the apical and basal surfaces of the epithelial cells, respectively. We assume that the most relevant forces are due to compression/stretching of the upper and lower cell faces. If the cell patch is initially in a stress-free flat state, active myosin stresses are introduced by adding an additional surface tension term to the apical face of the cells. The energy E of each cell then reads

$$E(A^+, A^-) = C_M \rho_M A^{+2} + K(A^+ - A^0)^2 + K(A^- - A^0)^2 \qquad (1)$$

where A^+ and A^- denote the areas of the outer (contracting) and inner cell faces, A^0 is the stress-free reference area of each face, and K their stiffness in the absence of myosin. ρ_M is the myosin concentration and C_M a proportionality

constant. We note that the dimensionless ratio $M = C_M \rho_M / K$ alone determines the myosin-induced shape deformation. M can thus be understood as a dimensionless *contractility coefficient* that is proportional to the local myosin concentration. We make two additional assumptions. First, owing to the incompressibility of the cytoplasm, we assume a constant cell volume. Second, drawing on the results from [3], we assume that the cell is significantly stiffer against vertical compression than against horizontal, and treat the cell height as a fixed quantity h. Taken together, we derive the constraint equation

$$A^+ + A^- + \sqrt{A^+ A^-} = 3A^0 \tag{2}$$

From this result, we can determine the equilibrium shape of the patch for given value of M in terms of the equilibrium areas $\bar{A}^+$ and $\bar{A}^-$ that minimize Eq. (1). Reducing the geometry to its middle surface, we find that the initially flat patch effectively obtains a new, myosin-induced target curvature κ given by

$$\kappa(M) \approx \frac{\theta}{s} \tag{3}$$

with $\theta = \pi - 2\tan^{-1}\left[2h/(\sqrt{\bar{A}^-} - \sqrt{\bar{A}^+})\right]$ the angle between middle-surface normals of neighboring cells and $s = (\sqrt{\bar{A}^+} + \sqrt{\bar{A}^-})/2$ the distance between cell centers on the middle-surface (Fig. 4B, Main Text). Additionally, we introduce the stretching factor

$$\sigma(M) = \frac{s}{\sqrt{A^0}} \tag{4}$$

which represents the degree of contraction the myosin induces on the middle-surface.

2 Curvature and Metric Tensor Definitions

Let $\mathbf{S} = \boldsymbol{\Theta}(\eta_1, \eta_2)$ by a 2D parameterization of the embryo surface in $\mathbb{R}^3$. Adopting the convention in which Greek indices correspond run form 1 to 2, and Latin indices run form 1 to 3, the tangent vectors to this surface are given (Fig. 4A, Main Text) as

$$\mathbf{a}_\alpha = \partial_\alpha \boldsymbol{\Theta} \tag{5}$$

and the surface metric, also referred to as the first fundamental form of the surface, is

$$a_{\alpha\beta} = \mathbf{a}_\alpha \cdot \mathbf{b}_\beta \tag{6}$$

A surface element is thus defined as

$$d\omega = \sqrt{|\det(a_{\alpha\beta})|}\, d\eta_1 d\eta_2$$

The unit length normal vector can be expressed in terms of the surface tangent vectors as

$$\mathbf{n} = \frac{\mathbf{a_1} \times \mathbf{a}_2}{|\mathbf{a_1} \times \mathbf{a}_2|} \tag{7}$$

The second fundemental form, which characterizes the curvature of the surface, is defined as

$$b_{\alpha\beta} = \mathbf{n} \cdot \partial_\beta \mathbf{a}_\alpha \tag{8}$$

For the purposes of this paper, we refer to the fundamental forms of the initial, undeformed ellipsoidal shell as $\overset{\circ}{a}_{\alpha\beta}$ and $\overset{\circ}{b}_{\alpha\beta}$. In order to capture the effect of the myosin-induced active stresses on local geometry, we define a second set of fundamental forms, $\bar{a}_{\alpha\beta}$ and $\bar{b}_{\alpha\beta}$, defined as

$$\bar{a}_{\alpha\beta} = \frac{1}{\sigma(M)} \overset{\circ}{a}_{\alpha\beta} \tag{9}$$

$$\bar{b}_{\alpha\beta} = \frac{\kappa(M)}{\sigma(M)} \overset{\circ}{a}_{\alpha\beta} \tag{10}$$

where the functions $\sigma(M)$ and $\kappa(M)$ are the contraction and curvature as a function of the local value of M, as derived in the previous section. Defined as such, these fundamental forms assign to each point on the surface a preferred isotropic contraction and curvature of the midplane. We note that for the myosin profiles studied in this work, $\sigma(M) \sim 1$ with a maximum deviation of $\sim 5\%$. We thus in the following set $\sigma \equiv 1$ and, consequently, can identify $\bar{a}_{\alpha\beta} = \overset{\circ}{a}_{\alpha\beta}$.

3 Energy Functional

Armed with the fundamental forms of our reference configuration defined above, we extend the classical Koiter shell (KS) energy functional of thin elastic shells to incorporate myosin-induced active stresses. The KS model describes the equilibrium of a thin shell when the thickness is small compared to its curvature [4]. The KS functional used here can be written as

$$\mathcal{E}_{KS} = \mathcal{E}_b + \mathcal{E}_s + \mathcal{E}_f \tag{11}$$

with the energy contribution from bending given as

$$\mathcal{E}_b = \frac{Yh^3}{24(1-\nu^2)} \int_{\bar{\omega}} S(M) \left[(1-\nu) \mathrm{Tr}[(b_{\alpha\beta} - \bar{b}_{\alpha\beta})^2] + \nu \mathrm{Tr}(b_{\alpha\beta} - \bar{b}_{\alpha\beta})^2 \right] d\bar{\omega} \tag{12}$$

the contribution from stretching

$$\mathcal{E}_s = \frac{Yh}{8(1-\nu^2)} \int_{\bar{\omega}} S(M) \left[(1-\nu) \mathrm{Tr}[(a_{\alpha\beta} - \bar{a}_{\alpha\beta})^2] + \nu \mathrm{Tr}(a_{\alpha\beta} - \bar{a}_{\alpha\beta})^2 \right] d\bar{\omega} \tag{13}$$

and energy contributions due to constraint forces

$$\mathcal{E}_f = \mu_V (V - V_0)^2 + \mu_S \int_{\bar{\omega}} B(\mathbf{\Theta}) \mathrm{d}\bar{\omega}$$

In Eqs. (12) and (13), Y is the Young's modulus, ν the Poisson ratio (we set $\nu = 1/2$ corresponding to an incompressible material), and the integral extends over the surface $\bar{\omega}$. The parameter S accounts for spatially dependent stiffness variations and is typically set to $S = 1$ for passive equilibrium materials. However, when including apical constriction stresses, S becomes myosin dependent: based on our toy model, we define $S = 1 + M$.

Eqs. (12) and (13) represent the energy cost of deviations of the actual membrane shape, characterized by the fundamental forms $a_{\alpha\beta}$ and $b_{\alpha\beta}$, from the reference configuration defined by $\bar{a}_{\alpha\beta}$ and $\bar{b}_{\alpha\beta}$. It is important to note that, while the initial configuration given by $\overset{\circ}{a}_{\alpha\beta}$ and $\overset{\circ}{b}_{\alpha\beta}$ is a simple ellipsoid, the reference configuration described by these tensors cannot be embedded in physical space for a general contractility distribution $M(\eta_1, \eta_2)$ [6]. This signifies that, in the presence of active stresses, the minimum energy configuration of our system will not necessarily be stress-free [1].

The constraint forces present in Eqn. (14) are two fold. The first term represents the volume constraint imposed by the enclosed yolk, treated here as a quadratic function of the deviation between the current volume V and the volume V_0 enclosed by the initial ellipsoid configuration. The second term represents the boundary wall constraint imposed by the vitelline membrane on the embryo. The vitelline membrane is assumed to be a rigid ellipsoid with the same dimensions as the initial embryo configuration. $B(\mathbf{\Theta})$ is a quadratic local contact energy, corresponding to a repulsive contact interaction between the epithelial membrane and the vitelline membrane. The constraint strength parameters μ_V and μ_S were set sufficiently large that very small deviations against constraints would produce energy costs on the order of the total stretching and bending contributions.

We numerically solve for equilibrium configurations of the energy Eq. (11) by the finite element method. To this end, we triangulate the epithelial surface by typically $N \sim 4 \cdot 10^4$ triangular subdivision surface finite elements [2, 5] with $\sim 2 \cdot 10^4$ nodes. By taking the gradient of Eq. (11), we obtain generalized forces acting at each node in the mesh. We supplement the resulting equations of motions with viscous damping, and integrate in time until an equilibrium configuration is found.

References

[1] Alain Goriely, Mark Robertson-Tessi, Michael Tabor, and Rebecca Vandiver. *Elastic Growth Models.* In Mathematical Modelling of Biosystems: 1-44, 2008. Springer Berlin Heidelberg.

[2] Fehmi Cirak, Michael Ortiz and Peter Schröder. *Subdivision surfaces: A new paradigm for thin-shell finite-element analysis.* International Journal for Numerical Methods in Engineering, 47(12): 20392072, 2000.

[3] Oleg Polyakov, Big He, Michael Swan, Joshua W Shaevitz, Matthias Kaschube and Eric Wieschaus. *Passive mechanical forces control cell-shape change during Drosophila ventral furrow formation.* Biophysical Journal, 107(4): 998-1010, 2014.

[4] Philippe G. Ciarlet. *An Introduction to Differential Geometry With Applications to Elasticity.* Journal of Elasticity, 78(1-3): 1-215, 2005.

[5] Roman Vetter, Norbert Stoop, Thomas Jenni, Falk K Wittel, and Hans J. Herrmann. *Subdivision Shell Elements with Anisotropic Growth.* International Journal for Numerical Methods in Engineering, 95(9): 791-810, 2013.

[6] Shahaf Armon, Efi Efrati, Raz Kupferman, and Eran Sharon. *Geometry and mechanics in the opening of chiral seed pods.* Science, 333(6050): 1726–1730, 2011